Structural Eng. / Earthquake Eng. Vol. 3. No. 1, 45 s-52 s, April 1986
Japan Society of Civil Engineers (Proc. of JSCE No. 368/ I -5)

AN AXISYMMETRIC JOINT ELEMENT UNDER NON-AXISYMMETRIC LOADINGS IN SEMI-ANALYTICAL FINITE ELEMENT METHOD

By Tameo KOBORI and Yasuo CHIKATA***

A new axisymmetric joint element model for semi-analytical finite element analysis of axisymmetric bodies subjected to non-axisymmetric loading is proposed. The new joint element model for axisymmetric interface has three degrees of freedom : normal, tangential and circumferential directions, and describes debonding (normal direction), and slip (tangential and circumferential direction) on the interface. The new joint element model was incorporated into a finite element program and test-case analyses were performed. The results indicate that the new joint element model is useful in the semi-analytical finite element analysis for deeper understanding of stress distributions on the axisymmetric interface.

1. INTRODUCTION

For the finite element analysis of the ground-footing system or cracked rock mass in which discontinuities are embedded in continuous system, a kind of interface element model which is called 'joint element' is often used. A simple and useful joint element model was formulated by Goodman et al.[1] for plane problem. The joint element describes the physical behavior of the system such as debonding and slip along the discontinuity.

In the finite element analysis of the ground-footing system or ground-pile system, the system is often modelled as axisymmetric bodies in cylindrical coordinate system, and hence, a new joint element model for axisymmetric interface is needed for modelling the discontinuities. Some joint elements for axisymmetric interface were formulated by Ghaboussi et al[2]., Heuze et al[3]., and Sasaki et al[4]., but these are adoptable only for axisymmetric problems. In the finite element analysis of the ground-footing system etc., which is modelled in cylindrical coordinate system, semi-analytical finite element procedure is usually adopted in the case that the system is subjected to non-axisymmetric loading, but a joint element for the case has not yet been formulated.

In this paper, a new axisymmetric joint element is proposed. The new joint element is conveniently used in the semi-analytical finite element analysis of axisymmetric bodies subjected to non-axisymmetric loading.

* Member of JSCE, Dr. Eng., Professor, Department of Civil Engineering, Kanazawa University (Kodatsuno 2-40-20 Kanazawa 920)
** Member of JSCE, M. Eng., Research Associate, Department of Civil Engineering, Kanazawa University (Kodatsuno 2-40-20 Kanazawa 920)

2. SEMI-ANALYTICAL FORMULATION[5)]

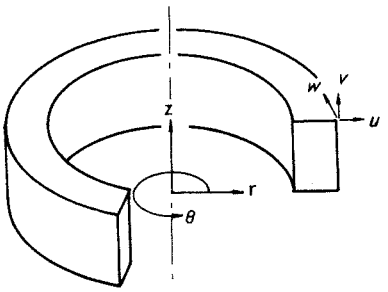

Fig. 1 Axisymmetric solid and related coordinate system.

The axisymmetric body is idealized as an assemblage of quadrilateral rings connected at their nodal circles. The displacements of nodes are represented in cylindrical coordinates by three components in radial (r), vertical (z), and circumferential (θ) directions (see Fig. 1). These displacement components are expressed by polynomials in the meridional plane, (r, z), as well as by a Fourier series in the circumferential direction, θ. Using the finite element formulation, it is assumed that the shape functions defining the variations of displacement, $\boldsymbol{u}$, can be written for the case that the non-axisymmetric load is symmetric about a plane containing the axis of revolution ($\theta=0$ plane), in a form of the superposition of M harmonics :

$$\boldsymbol{u}=\boldsymbol{N}(r,z)\left(\boldsymbol{u}_0+\sum_{m=1}^{M}\boldsymbol{C}_m\boldsymbol{u}_m\right) \quad (1)$$

where,

$\boldsymbol{u}=\{u\ v\ w\}^T$: displacements in r, z and θ direction

$\boldsymbol{N}$: shape functions matrix

$\boldsymbol{C}_m=\mathrm{diag}[C_m\ C_m\ S_m\ C_m\ C_m\ S_m\ C_m\ C_m\ S_m\ C_m\ C_m\ S_m]$: for 4 nodes element

The vectors $\boldsymbol{u}_0, \boldsymbol{u}_m$ stand for the sets of appropriate nodal values coefficients of the Fourier representations.

Similarly, the loading terms have the form

$$\boldsymbol{f}=\boldsymbol{f}_0+\sum_{m=1}^{M}\boldsymbol{C}_m\boldsymbol{f}_m \quad (2)$$

where,

$\boldsymbol{f}=\{f_r\ f_z\ f_\theta\}^T$

With restriction to small strain and small displacements the strain in cylindrical coordinates is given by

$$\begin{aligned}\{\varepsilon\}&=\{\varepsilon_r\ \varepsilon_z\ \varepsilon_\theta\ \gamma_{rz}\ \gamma_{r\theta}\ \gamma_{z\theta}\}^T\\&=\left\{\frac{\partial u}{\partial r},\frac{\partial v}{\partial z},\frac{u}{r}+\frac{1}{r}\frac{\partial w}{\partial\theta},\frac{\partial u}{\partial z}+\frac{\partial v}{\partial r},\frac{1}{r}\frac{\partial u}{\partial\theta}+\frac{\partial w}{\partial r}-\frac{w}{r},\frac{1}{r}\frac{\partial v}{\partial\theta}+\frac{\partial w}{\partial z}\right\}^T\\&=\boldsymbol{B}\boldsymbol{u}=[\boldsymbol{B}^0,\boldsymbol{B}^1,\cdots,\boldsymbol{B}^M]\{\boldsymbol{u}_0,\boldsymbol{u}_1,\cdots,\boldsymbol{u}_M\}^T\end{aligned} \quad (3)$$

For the i-th node, the strain matrix $\boldsymbol{B}_i^m$ is determined as follows :

$$\boldsymbol{B}_i^m=\mathrm{diag}[C_m\ C_m\ C_m\ C_m\ S_m\ S_m]\cdot\begin{bmatrix}\partial N_i/\partial r & 0 & 0\\ 0 & \partial N_i/\partial z & 0\\ N_i/r & 0 & mN_i/r\\ \partial N_i/\partial z & \partial N_i/\partial r & 0\\ -mN_i/r & 0 & \partial N_i/\partial r-N_i/r\\ 0 & -mN_i/r & \partial N_i/\partial z\end{bmatrix} \quad (4)$$

The finite element formulation can now follow the standard pattern[6)]. The stiffness matrix will now be written listing the contributions of each harmonic separately. A typical submatrix of an element stiffness matrix $\boldsymbol{K}$ is written as

$$\begin{aligned}\boldsymbol{K}_{ij}^{lm}&=\int_{Vol}(\boldsymbol{B}_i^l)^T\boldsymbol{D}\boldsymbol{B}_j^m d(Vol)\\&=\int_0^{2\pi}\int_S(\boldsymbol{B}_i^l)^T\boldsymbol{D}\boldsymbol{B}_j^m r\,dr\,dz\,d\theta \qquad (l,m=0,1,\cdots M)\end{aligned} \quad (5)$$

where $\boldsymbol{D}=\boldsymbol{D}(r,z)$ only.

And because of the orthogonality of trigonometric function, the followings are derived :

$$K_{ij}^{lm}=0 \text{ for } l \neq m \quad (6)$$

Thus a decoupled form is obtained as

$$\begin{bmatrix} K^0 & \cdots & 0 & \cdots & 0 \\ \vdots & & & & \vdots \\ 0 & \cdots & K^m & \cdots & 0 \\ \vdots & & & & \vdots \\ 0 & \cdots & 0 & \cdots & K^M \end{bmatrix} \begin{Bmatrix} u_0 \\ \vdots \\ u_m \\ \vdots \\ u_M \end{Bmatrix} = \begin{Bmatrix} f_0 \\ \vdots \\ f_m \\ \vdots \\ f_M \end{Bmatrix} \quad (7)$$

in which $M+1$ separate problems are solved for u_m unknowns.

The formulation described above can be easily extended to the cases that the load is anti-symmetric or combination of axisymmetric and anti-symmetric about $\theta=0$ plane.

3. FORMULATION OF NEW AXISYMMETRIC JOINT ELEMENT

The joint element formulated by Goodman et al.[1] for plane problem is advanced to the one for semi-analytical analysis of three dimensional problem in cylindrical coordinate system.

The new joint element has a meridional plane which consists of pairs of nodal lines 1-4 and 2-3. In the initial state, the pairs of nodal lines 1-4 and 2-3 have same coordinates. Notations for the new joint element are shown in Fig. 2.

The behavior of the axisymmetric interface which is modelled by the joint element, is described by the relationship of relative displacements between two circular plates 1-2 and 3-4 in Fig. 2. The components of the behavior are debonding (normal (η) direction to the interface plane), and slip (tangential (ξ) or circumferential (θ) direction).

The relative displacements between a pair of circular plates 1-2 and 3-4 are written as follows :

$$\boldsymbol{d}=\{d_\xi\ d_\eta\ d_\theta\}^T=\boldsymbol{N}^*\boldsymbol{u}^*=[-N_1\boldsymbol{I}\ -N_2\boldsymbol{I}\ N_2\boldsymbol{I}\ N_1\boldsymbol{I}]\boldsymbol{u}^* \quad (8)$$

in which,

$\boldsymbol{u}^*=\{u_1^*\ v_1^*\ w_1^*\cdots u_4^*\ v_4^*\ w_4^*\}^T$

: displacements of nodal lines in ξ, η and θ direction

$N_1=(1-2\xi/L)/2$, $N_2=(1+2\xi/L)/2$: shape functions

$\boldsymbol{I}$: 3×3 unit matrix

L : joint length in (r, z) plane (see Fig. 2)

The stress-displacement relationship is written as

$$\boldsymbol{P}=\boldsymbol{k}\boldsymbol{N}^*\boldsymbol{u}^* \quad (9)$$

in which

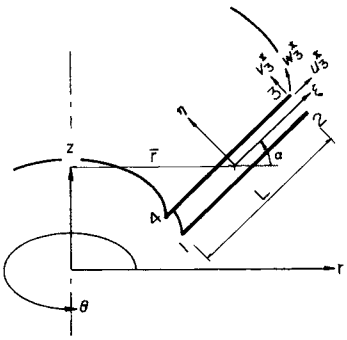

Fig. 2 Notations for joint element.

$\boldsymbol{P}=\{P_\xi\ P_\eta\ P_\theta\}^T$: stresses in a joint element and,

$$\boldsymbol{k}=\begin{bmatrix} k_\xi & 0 & 0 \\ 0 & k_\eta & 0 \\ 0 & 0 & k_\theta \end{bmatrix} \quad (10)$$

: element stiffness per unit length

According to the semi-analytical formulation, relative displacement vector $\boldsymbol{d}$ is rewritten as follows :

$$\boldsymbol{d}=\boldsymbol{N}^*\sum_{m=0}^{M}\boldsymbol{C}_m\boldsymbol{u}_m^* \quad (11)$$

where,

$\boldsymbol{u}_m^*$ is the coefficients vector of nodal displacements in the Fourier series form.

Then the element stiffness matrix for m-th harmonic becomes

$$\boldsymbol{K}_m=\int_0^{2\pi}\int_{-L/2}^{L/2}(\boldsymbol{N}\boldsymbol{C}_m)^T\boldsymbol{k}\boldsymbol{N}\boldsymbol{C}_m r\,d\xi\,d\theta \quad (12)$$

Evaluating $\boldsymbol{K}_m$ at the element centroid, Eq. (13) is obtained.

$$K_m=\frac{\pi\bar{r}L}{4}\begin{bmatrix} k & k & -k & -k \\ k & k & -k & -k \\ -k & -k & k & k \\ -k & -k & k & k \end{bmatrix} \quad \cdots\cdots (13)$$

where, $\bar{r}=(r_1+r_2+r_3+r_4)/4$.

For 0-th harmonic, the constant $\pi\bar{r}L/4$ is replaced by $2\pi\bar{r}L/4$, and in this case ($m=0$), eliminating the columns and rows about θ-axis component, K_0 is identical to the element stiffness matrix for the axisymmetric joint element formulated by Heuze et al.[3]. For the case $m\geqq 1$, K_m is independent of the harmonic order m.

As seen in the formulation described above, the joint element has the three components of behavior for $m=1$ (see Fig. 3).

If the global coordinate system does not coincide with the local system, K_m should be rotated in a following transformation.

$$K_m^G=T^T K_m T, \quad K_m^G : \text{in global coordinates} \quad \cdots\cdots (14)$$

$$T=\begin{bmatrix} t & 0 & 0 & 0 \\ 0 & t & 0 & 0 \\ 0 & 0 & t & 0 \\ 0 & 0 & 0 & t \end{bmatrix}, \quad t=\begin{bmatrix} \cos\alpha & \sin\alpha & 0 \\ -\sin\alpha & \cos\alpha & 0 \\ 0 & 0 & 1 \end{bmatrix}$$

The rotation angle α is defined in Fig. 2.

The constitutive relation between the stresses in the joint element is assumed as illustrated in Fig. 4. This is an extension of the constitutive relation proposed by Toki et al.[7]. Fig. 4(a) illustrates the constitutive relation between the stress and displacement in the normal (η) direction to the joint plane. Fig. 4(b) shows the constitutive relations between the stresses in tangential (ξ) and circumferential (θ) direction. The specification whether debonding or slip has occurred or not, is made based on the stresses at the element centroid. Stresses at the element centroid in the local system are given as follows (see Eq. (9)) :

$$\begin{Bmatrix} \tau_\xi \\ \sigma \\ \tau_\theta \end{Bmatrix} = 0.5 \begin{Bmatrix} k_\xi(-u_1^*-u_2^*+u_3^*+u_4^*) \\ k_\eta(-v_1^*-v_2^*+v_3^*+v_4^*) \\ k_\theta(-w_1^*-w_2^*+w_3^*+w_4^*) \end{Bmatrix} \quad \cdots\cdots (15)$$

When $\sigma>0$ (tension), it means debonding has occurred, and then stresses are released in a joint element. When $\sigma\leqq 0$ (compression) and $|\tau_\xi|>|\tau_y|$, it means slip has occurred along ξ direction, and then $|\tau_\xi|$ must be reduced to $|\tau_y|$. τ_y is the yield tangential shear stress. For θ direction, the same specification for ξ direction is made, and then, τ_y stands for the yield circumferential shear stress. The yield shear stress τ_y is assumed to follow Mohr-Coulomb yield criteria, i.e. :

$$\left.\begin{array}{ll} \tau_y=C-\sigma\tan\varphi & (\sigma\leqq 0) \\ \tau_y=0 & (\sigma>0) \end{array}\right\} \quad \cdots\cdots (16)$$

Where C denotes cohesion, and φ denotes friction angle respectively.

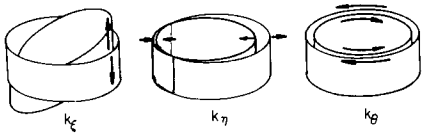

Fig. 3 Schematic of modes of deformation at interface ($m=1$).

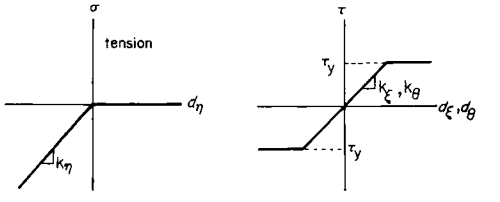

(a) Normal direction (b) Tangential and circumferential direction

Fig. 4 Load deflection curve.

If $M+1$ (from 0-th to M-th harmonics) Fourier coefficients have been used in the expansion of the applied load, the following procedure is adopted[5),8),9)].

(1) Solve $M+1$ separate sets of equation to obtain the nodal displacement corresponding to each harmonic.

(2) The stresses at the centroid of the joint element and at each Gauss point for other element are calculated from the nodal displacement corresponding to each harmonics.

(3) The stresses for each harmonics are combined to get the total stresses on any meridional plane, and added to the values of previous iteration stage.

(4) Check whether debonding or slip has occurred or not for each joint element. If debonding or slip has occurred, the stress is reduced on a interface. At the same time, the internal nodal force is calculated by Eq. (2).

(5) Check the convergence on some meridional plane. The convergence criterion is as follows

$$\mathbf{F}^r / \mathbf{F}_f < \varepsilon \quad \cdots\cdots (17)$$

This convergence criterion indicates that convergence occurs if the norm of the residual forces at r-th iteration stage ($\mathbf{F}^r$) becomes less than ε times of the norm of the total applied forces ($\mathbf{F}_f$).

In the procedure described above, the joint stiffness is not reduced after debonding or slip has occurred, because the semi-analytical technique requires the constant properties in the circumferential direction. So the stress transfer method[10)] is adopted with initial stiffness.

4. EXAMPLES

The connection between pile-head and footing subjected to horizontal load at pile end, shown in Fig. 5, is chosen to show a practical application of the new joint element. The pile-head has both horizontal and vertical interfaces with the footing. Let debonding or slip occur only on the vertical interface. The finite element mesh is shown in Fig. 6. The applied lateral load is transformed into shear force and moment as shown in Fig. 6.

Mechanical properties of pile, footing and joint element are listed in Table 1.

As shown in Table 1, analyses were performed for 3 cases. Case-1 and case-3 are the extreme cases. In case-1, only debonding occurs on the interface (so, slip does not occur) as the result of calculation, and in case-3, the interface is fric-

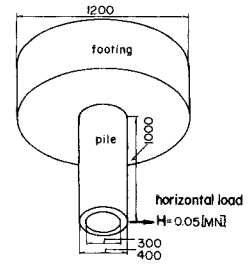

Fig. 5 Connection between pile-head and footing.

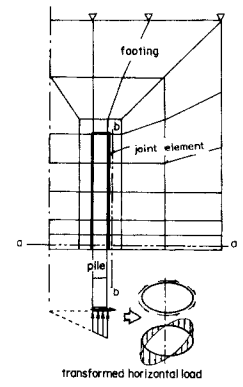

Fig. 6 Finite element mesh.

Table 1 Mechanical properties.

		case-1	case-2	case-3
Pile, Footing	Young's modulus E	2.0×10^4 (MPa)	2.0×10^4 (MPa)	2.0×10^4 (MPa)
	Poisson ratio ν	0.17	0.17	0.17
Joint	k_ξ	1.0×10^4 (MPa/m)	1.0×10^4 (MPa/m)	1.0×10^4 (MPa/m)
	k_η	2.0×10^4 (MPa/m)	2.0×10^4 (MPa/m)	2.0×10^4 (MPa/m)
	k_θ	1.0×10^4 (MPa/m)	1.0×10^4 (MPa/m)	1.0×10^4 (MPa/m)
	C	2.0 (MPa)	0.5 (MPa)	0.0 (MPa)
	φ	30°	30°	0°

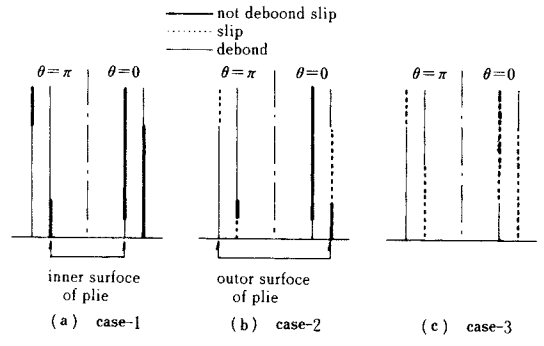

Fig. 7 Debonding or slip region.

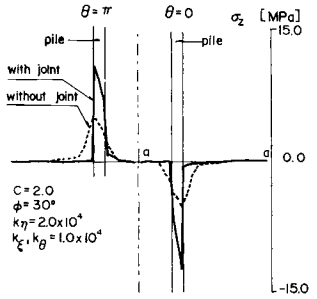

Fig. 8 Profiles of vertical stress on cross section a-a (case-1).

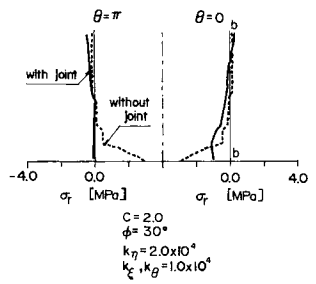

Fig. 9 Profiles of horizontal stress on cross section b-b (case-1).

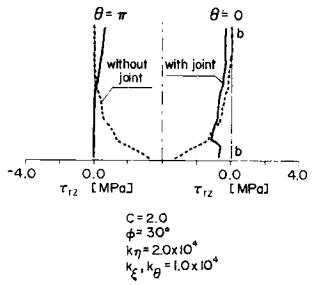

Fig. 10 Profiles of shear stress on cross section b-b (case-1).

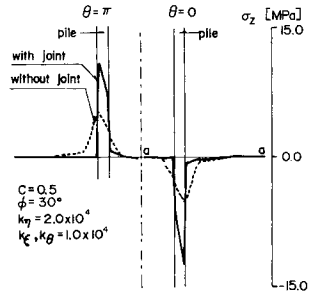

Fig. 11 Profiles of vertical stress on cross section a-a (case-2).

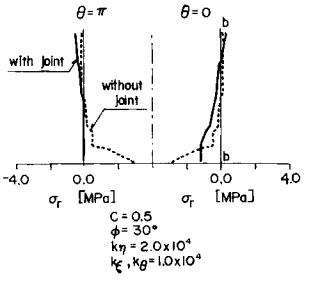

Fig. 12 Profiles of horizontal stress on cross section b-b (case-2).

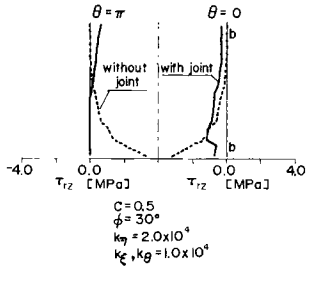

Fig. 13 Profiles of shear stress on cross section b-b (case-2).

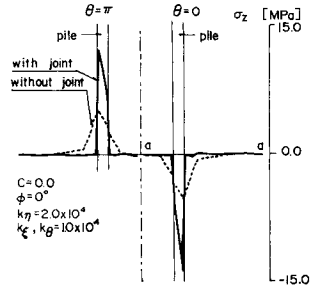

Fig. 14 Profiles of vertical stress on cross section a-a (case-3).

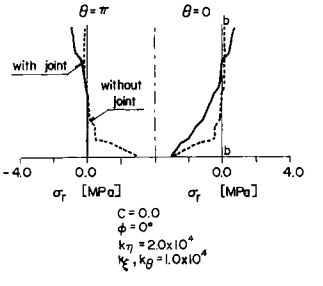

Fig. 15 Profiles of horizontal stress on cross section b-b (case-3).

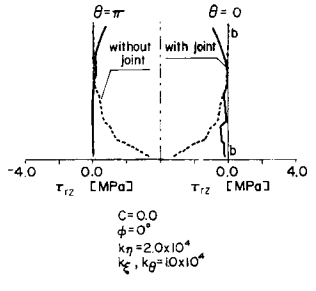

Fig. 16 Profiles of shear stress on cross section b-b (case-3).

tionless. The characteristics of the joint elements in these cases are specified by cohesion C and internal friction angle φ.

The adopted tolerance value of ε is 0.03 (3%), for convergence check.

The judgement wherther debonding or slip has occurred or not, is made in five planes : $\theta=0$, $\pi/4$, $\pi/2$, $3\pi/4$ and π, respectively.

The calculated results are shown in Figs. 7-16.

Figs. 7(a)-(c) show the region (=joint element) at which debonding or slip has occurred corresponding to the cases 1-3, respectively.

In Fig. 8, Fig. 11 and Fig. 14, profiles of σ_z distribution on a cross section a-a are shown, corresponding to case-1, case-2 and case-3, respectively. And in Fig. 9, Fig. 12 and Fig. 15, profiles of σ_r distribution on a cross section b-b are shown, corresponding to case-1, case-2 and case-3, respectively. Similary in Fig. 10, Fig. 13 and Fig. 16, profiles of τ_{rz} distribution on a cross section b-b are shown, corresponding to

case-1, case-2 and case-3, respectively (cross sections a-a and b-b are shown in Fig. 5). And in Figs. 8-16, the calculated results are compared with the results for the case that the pile and footing are modelled as a continuum without joints.

Comparing the results in cases with the joint and without the joint, in Figs. 8, 11 and 14, the distributions of σ_z are discontinuous on the side face of pile, because debonding has occurred on the external side of pile ($\theta=\pi$ plane) as well as on the internal side of pile ($\theta=0$ plane). The effect of the friction in the interface is seen in comparison between Fig. 8 and Fig. 14 (on the external side of pile in $\theta=0$ plane and on the internal side of pile in $\theta=\pi$ plane).

The effect of friction in the interface on the stress propagation is seen clearly in Fig. 9, Fig. 12 and Fig. 15 ($\theta=0$ plane). And also, σ_r distribution shows leverage support.

Figs. 10, 13 and 16 also show the effect of the friction in the interface crearly. In Figs. 10 and 13, τ_{rz} is propagated on $\theta=0$ plane. On the contrary, in Fig. 16 on $\theta=0$ plane, τ_{rz} is not propagated because the interface is frictionless.

Fig. 17 shows the convergence path for the 2 cases : $C=2.0$, $\varphi=30$ (case-1), and $C=0.0$, $\varphi=0$ (case-3). The norm of residual sum ratio (value of the left parenthesis of Eq. (17)) decreases rapidly to about 20 %, but thereafter the ratio of (decrease)/(iteration) becomes smaller. The convergence has achieved more rapidly for the case that slip does not occur on the interface (case-1) compared with the case that the joint is frictionless (case-3).

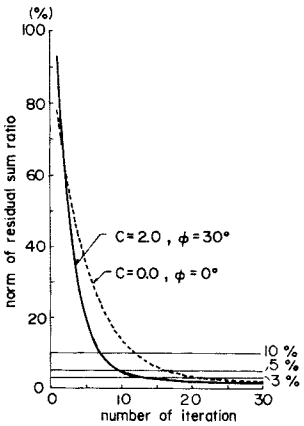

Fig. 17 Prosesses of convergence.

For the case that the stiffness of pile is rather larger than that of footing (Young's modulus : pile=2.0×10^5, footing=2.0×10^4 MPa, $k_\eta=2.0\times10^5$, $k_\xi=k_\theta=1.0\times10^5$ MPa/m, other conditions are same as case 3), the result is almost same as the result of case-3.

The appropriate number of adopted Fourier harmonics M(0-th to M-th) is variable according to the applied load. For the example showed above, $M=4$ is sufficient because the result of the case with $M=4$ almost coincides with the result of the case with $M=8$.

It is one of the important problems to find the appropriate value of the joint stiffness. In the example showed above (case-3), set the joint stiffness higher value $k_\eta=2.0\times10^5$, $k_\xi=k_\theta=1.0\times10^5$, then the number of iterations for convergence has increased, and the final results of stresses have also increased. In order to check whether the value of the joint stiffness is appropriate or not, further investigations are needed but are not made here. Toki et al.[7] set the value of the joint element stiffness equal to the value of the solid element stiffness next to the joint, but in the case that the stress transfer method is adopted, it seems rather larger value for get convergence in small iteration number.

5. CONCLUSIONS

The joint element for plane problem which was formulated by Goodman et al., has been extended to the model for axisymmetric interface.

This new joint element model is applicable in the semi-analytical finite element analysis of axisymmetric bodies with discontinuities subjected to non-axisymmetric loading.

The new joint model was incorporated into a finite element program[9),11)] and test-case analyses were performed. The results indicate that the use of the new joint element model lead to a better understanding of stress distribution on the axisymmetric interface.

ACKNOWLEDGEMENT

The numerical computation for this study has been performed on the FACOM M-170 F computer system

of the Data Processing Center, Kanazawa University.

REFERENCE

1) Goodman, R. E., Taylor, R. L. and Brekke, T. L. : A model for mechanics of joint rock, Proc. of ASCE, Vol. 94, SM 3, pp. 637~659, 1968.
2) Ghaboussi, J., Wilson E. L. and Isenberg, J. : Finite element for rock joints and interfaces, Proc. of ASCE, Vol. 9, SM 10, pp. 833~849, 1973.
3) Heuze, R. E. and Barbour, T. G. : New models for rock joints and interfaces, Proc. of ASCE Vol. 108, pp. 757~776, 1982.
4) Sasaki, M. and Nakai, T. : Finite element analysis of the pile with surface-friction, Proc. of 37 th Annual Meeting of JAPAN SOCIETY OF CIVIL ENGINEERING (JSCE), Ⅲ-245, pp. 487~488, 1982. (in Japanese)
5) Winnicki, L. A. and Zienkiewicz O. C. : Plastic (or visco-plastic) behavior of axisymmetric bodies subjected to non-symmetric loading semi-analytical finite element solution, Int. J. Numerical Meth. Engng., Vol. 14, pp. 1399~1412, 1979.
6) Zienkiewicz, O. C. : The Finite Element Method, McCraw-Hill, London, 1977.
7) Toki, K., Satoh, T. and Miura, F. : Separation and sliding between soil and structure during strong ground motion, Proc. of JSCE, No. 302, pp. 31~41, 1980. (in Japanese)
8) Thomas, T. J., Nair, S. and Vijay K. Garg : Elasto-plastic stress analysis and fatigue life prediction of a freight car wheel under mechanical and cyclic thermal loads : Int. J. Computers & Structures, Vol. 17, pp. 313~320, 1983.
9) Owen, D. R. J. and Hinton, E. : Finite Elements in plasticity-theory and practice-, pp. 157~269, Pineridge Press, 1980.
10) Zienkiewicz, O. C., Valliappan, S. and King, I. P. : Stress Analysis of Rock as a 'No Tension' Material, Geotechnique, Vol. 18, pp. 56~66, 1968.
11) Kobori, T. and Yoshida, H. : Programs for structural analysis by finite element method, pp. 218~220, 251~257, Maruzen, 1980. (in Japanese)

(Received April 12 1985)